

Bose–Einstein Condensate Dark Matter Model with Three-Particle Interaction and Two-Phase Structure

A.M. Gavrilik*, M.V. Khelashvili, A.V. Nazarenko
*Bogolyubov Institute for Theoretical Physics of NAS of Ukraine,
 14b, Metrohichna Str., Kyiv 03143, Ukraine*

(Dated: February 1, 2022)

We explore the consequences of including the repulsive three-particle interaction in the model of Bose–Einstein condensate dark matter model or fuzzy dark matter. Such a model based on properly modified Gross–Pitaevskii equation is intended to describe the distribution of dark matter particles in the highly dense regions, which correspond to the galaxy core and/or to the overlap of colliding galaxies. Specifically, we deal with the ϕ^6 -model in terms of the macroscopic wave function of the condensate, where a locality of interaction is guaranteed by a large correlation length assumed to hold. After calculation of main thermodynamical characteristics, we find strong evidence of the existence of two distinct phases of dark matter, within its core, separated by the instability region lying between two differing special values of the pressure acting in the model. Some implications stemming from the existence of two phases and the related first-order phase transition are discussed.

PACS numbers: 95.35.+d, 03.75.Hh, 05.70.Ce, 05.70.Fh

Keywords: dark matter, galactic halo, core, BEC, first-order phase transition

I. INTRODUCTION

The notion of dark matter (DM), though being rather old one [1, 2], is a widely accepted concept nowadays. A support in favor of its existence stems from both gravitational-lensing observation and the data on galaxy rotation curves. But, despite a vast amount of theoretical (and experimental) studies, the ultimate nature of DM remains still unknown.

In the last two decades or more, among a diversity of approaches to DM, ever-increasing attention is focused on a class of DM models known as Bose-Einstein condensate (BEC) dark matter (also named “fuzzy DM” or FDM, “quantum wave-function DM” or ψ DM models, scalar-field dark matter, ultralight dark matter), see [3–5] as well as the reviews [6–11] with numerous references therein. Also, superfluid dark matter models [12, 13] are closely related to this class.

Main point/feature of this class of models is that DM constitutes a BEC subjected to a long range correlation. There are some variations within this class, depending on (i) the sort and the values of mass of fuzzy DM constituents, ranging from 10^{-32} eV to 10^{-21} eV and even higher in some cases, and on (ii) whether self-interactions are neglected [3, 5] or the DM particles experience some repulsive self-interaction, small or not, quartic [14, 15] or more complex. (The case with neglected self-interactions is the most restrictive one and requires the mass of FDM to be 10^{-22} eV for the DM core stability; on the other hand, more freedom is admitted when certain self-interactions are taken into account.) Among the explored self-interactions we encounter, besides the most popular quartic one, also the logotropic [16], cos- and cosh-type

ones [17–20]. The studies of the role of diverse (orders, attractive/repulsive cases of) self-interactions of ultralight scalar DM particles are of utmost importance.

The FDM class surpasses the cold dark matter models (CDM) models [21] in the sense that it succeeds to resolve those problems of CDM that appear at the small (i.e. galactic or subgalactic) scales. In particular, it was shown that the BEC DM scenario of DM, exploiting Gross–Pitaevskii (GP) equation related with quartic term in the self-interaction scalar potential, jointly with the Poisson equation, enable to overcome [22, 23] the well-known cusp/core problem of CDM models. Besides, the intrinsic tools of the BEC DM models are efficient enough to properly treat the gravitational collapse [24] issue of the BEC dark matter halos, see e.g. [20, 25]. The very important observational realm of distribution of dark matter in galaxies [26] and the galactic rotation curves can as well be described with very good agreement [15, 25, 27–32, 42]. In a number of works, the BEC DM predictions are tested with the galaxies kinematic observations using galaxies of diverse morphologies. It starts from studying of ultracompact dwarf (UCD) galaxies [33], wherein the new scenario of UCD origin was proposed in the framework of BEC DM; or the sample of eight brightest dwarf spheroidal satellites of Milky Way, which was considered to constrain BEC halo size in the model of BEC DM within the Thomas–Fermi approximation [27]. The model was applied as well to the largest galaxies such as Milky Way, that together with 12 nearby dwarf galaxies from SPARC are used to test astrophysical effect of BEC DM halo rotation [28]. It is worth to mention that SPARC database of disk galaxies of Hubble type from H0 to Irr (note, the most of galaxies belongs to low surface galaxies class) is frequently used to compare BEC DM predictions with the observed galaxies kinematics. The samples of 12 dwarf galaxies from SPARC [29] and 139 galaxies of different types selected

*e-mail: omgavr@bitp.kiev.ua

from the database according to the data quality [30] are fitted well by the slowly rotating BEC DM model. Besides, the BEC DM with super-massive black hole in halo center was compared to NFW density profile by fitting of 20 SPARC galaxies with the desired accuracy of data [31], the both models describe the observations well, but it is not clear which of two models is preferred by the data.

In addition, FDM is believed to manage successfully the important theme of core mass-halo mass relation [20, 32, 34]. In general, the BEC approach to modeling DM, based on (modified versions of) the Gross–Pitaevskii–Poisson system, helps to describe the known and reveals possible new features or phenomena characteristic of DM core and halo.

It is worth to note that diverse types of Bose-like DM candidates (satisfying BEC paradigm) have been studied in the literature: besides the widely explored usual unspecified bosons, there are rather popular axions (with masses ranging from 10^{-20} eV to 1 eV) [35–39], the Stueckelberg bosons [40], or even the massive gravitons [41, 42] (for different bounds on graviton mass, see e.g. [43]). Moreover, in some recent papers, specific versions of deformed bosons (obeying statistics differing from the pure Bose one) are explored in the role of DM particles [44–47], and these are admitted thanks to the fact of existence of condensate phase analogous to usual BEC. Note that the description of galactic rotation curves obtained within the particular so-called μ -deformed approach turns out to be quite successful [46], even without taking into account the visible (baryonic) component of galaxies.

Recently, the interest is drawn to the role of six-order repulsive self-interaction term in the scalar potential within the BEC framework. Due to sextic term, the situation qualitatively changes [48]. In particular, this can lead to nontrivial phase structure of the core in the central part of the DM halo. Let us mention the work of Chavanis [17] which has demonstrated the existence of two phases — one “dilute” and the other “dense” — pictured through the mass-radius relation (note that this was done in the context of axion stars, with only short remark added that analogous features can occur in the system of axionic DM).

The goal of our paper is to explore main consequences of including the (repulsive) sextic self-interaction term in the potential of gravitating BEC dark matter model. The basic aspect of our study consists in dealing not with the system of Gross–Pitaevskii (GP) and Poisson equations, but with a single properly modified form of the GP equation in which the gravitational potential enters non-locally, through the action of inverse Laplacian. That suggests the extensive usage of numerical methods to study the density profiles of the BEC dark matter along with their stability properties. On their base, we are able to obtain the major thermodynamical functions of BEC DM. Detailed analysis of the latter, especially of their mutual dependencies, yields the most valuable information about the appearing phases (stable, metastable, and

unstable regions) and the presence of first-order phase transition.

The paper has the following structure: in Sec. 2, main arguments in favor of the adopted particular choice of the model are presented, with special attention to the role of sixth order repulsive self-interaction term in the potential of fuzzy or BEC dark matter. In Sec. 3, within the appropriately modified version of the Gross–Pitaevskii equation we treat the sextic self-interaction term jointly with (the potential of) gravitational interaction employed in a nonlocal fashion. Due to the latter circumstance, we deal with single equation instead of the nonlinear Schrödinger–Poisson system. As an important step of the whole analysis, we restrict ourselves with the Thomas–Fermi approximation (when, due to sending $\hbar \rightarrow 0$, kinetic term is eliminated). Then, the complete form of the model is explored in Sec. 4. Namely, with inclusion of quantum processes, the calculation of the relevant thermodynamical functions is performed. On this base, in Sec. 5 we establish the existence of, and analyze in detail, the two distinct phases that are realized in the dark matter core. The final section is devoted to discussion of implications, concluding remarks and outlook.

II. CONSTRUCTING A MODEL

In this Section, we present the criteria that allow us to formulate a model of dark matter (together with the conditions of its applicability), which we then further study. Our arguments stem from a comparison of empirical data for galaxies and the properties of some theoretical models of dark matter formed by Bose particles (and fields).

A. The Scaling Criterion for Interactions

As a kind of the criteria that justifies the ability of a theoretical model to describe observables, we use scaling reasonings. By implementing the scaling in practice, we intend to choose a more realistic model for our study.

Considering a sample of observed galaxies in a wide mass range, it allows us to relate core size r_0 and mass density ρ_0 in the center. Such a relation is found to be close to $\rho_0 \propto r_0^{-\beta}$ with $\beta \approx 1$. In fact, $\beta = 1.3$ for the studied galaxies sample. A close result is obtained in [49] from analysis of *dwarf spheroidal* galaxies, which gives a similar correlation between halo radius and mass density, that is, $\rho_0 \propto r_0^{-1.2}$.

Let us first review the scaling relations of *fuzzy dark matter* (FDM), where DM particles are described by complex-valued wave function $\psi(r)e^{-i\gamma t/\hbar}$ and individual mass m . Accordingly to FDM, stationary Schrödinger–Poisson equations are

$$\gamma\psi = -\frac{\hbar^2}{2m}\Delta\psi + mV_{\text{gr}}\psi, \quad \Delta V_{\text{gr}}(r) = 4\pi G\rho(r), \quad (1)$$

where Δ is a Laplace operator; $\rho = m|\psi|^2$.

The system possesses exact scaling symmetry with parameter λ :

$$r \rightarrow \lambda^{-1}r, \quad \rho \rightarrow \lambda^4\rho, \quad \psi \rightarrow \lambda^2\psi, \quad \gamma \rightarrow \lambda^2\gamma. \quad (2)$$

It leads to the scaling relation $\rho_0 \propto r_0^{-4}$ between DM halo radius r_0 and central density ρ_0 . As it is shown in [23], this relation strictly contradicts the observations. Indeed, $\beta = 4$ is far from $\beta = 1.3$ already noted above. Although, a realistic model should be applicable to the DM description, as is expected, for a large sample of galaxies, but not only exceptions.

An important conclusion results from the FDM model: In order to reach $\beta \simeq 1$ we need to take self-interaction among DM particles into account.

Including repulsive or attractive ψ^4 self-interaction into the FDM model, the scaling relation takes the form with $\beta = 2$ for a large range of disk size, that is close to the value derived in [23]. However, the solutions found are unstable and thus do not resolve the issue. Nevertheless, there is a possibility to obtain stable solutions in the required range of parameters, combining repulsive and attractive potentials in some way to prevent a halo collapse or outward flow of particles.

Continuing the analysis, let us now test ψ^6 -model in details. Clearly, the FDM equation with repulsive ψ^6 term does not obey the scaling symmetry (2) any more as well as any other scaling relations. Thus, it becomes more complicated to find relation between r_0 and ρ_0 .

We are forced to apply a hint, indicating that solution of problem can be found within the framework of ψ^6 -model. Following [39], we estimate the contribution of several terms to a total energy of halo using an exponential ansatz. This trick has already been used in the literature to study a stability of scalar field DM halos.

Thus, let the total energy E (in infinite volume, with its element $dV(r) = 4\pi r^2 dr$) and its density \mathcal{E} of spherically symmetric DM halo be

$$E = \int_0^\infty \mathcal{E}(r) dV(r), \quad \mathcal{E} = \mathcal{E}_q + \mathcal{E}_{\text{int}} + \mathcal{E}_{\text{gr}}, \quad (3)$$

where

$$\mathcal{E}_q = \frac{\hbar^2}{2m} \left| \frac{d\psi}{dr} \right|^2, \quad \mathcal{E}_{\text{int}} = \frac{U}{3} |\psi|^6, \quad \mathcal{E}_{\text{gr}} = \frac{1}{2} \rho V_{\text{gr}}. \quad (4)$$

The wave function ψ is normalized so as to give the total number of particles N :

$$N = \int_0^\infty |\psi(r)|^2 dV(r). \quad (5)$$

Further, we adopt the exponential ansatz for ψ :

$$\Phi(r) = \sqrt{\frac{N}{\pi r_0^3}} e^{-\frac{r}{r_0}}, \quad (6)$$

which satisfies (5).

This is a simple ansatz to simulate field behavior in the inner region when an exact solution is unknown. It is valid in the range of $r \lesssim r_s$ for some finite r_s , but breaks down in the outer region.

Substituting (6) instead of ψ into (3), one gets

$$E = a \frac{N}{r_0^2} + b \frac{N^3}{r_0^6} - c \frac{N^2}{r_0}, \quad (7)$$

$$a = \frac{\hbar^2}{2m}, \quad b = \frac{U}{81\pi^2}, \quad c = \frac{5Gm^2}{16}. \quad (8)$$

To calculate the action of operator Δ and its inverse on function $f(r)$ in the spherically symmetric case (what is needed for finding V_{gr}), it is enough to use their radial parts defined as

$$\Delta_r f(r) = \partial_r^2 f(r) + \frac{2}{r} \partial_r f(r), \quad (9)$$

$$\Delta_r^{-1} f(r) = -\frac{1}{r} \int_0^r f(s) s^2 ds - \int_r^R f(s) s ds. \quad (10)$$

where R is radius of the ball, where the matter is located. We put $R \rightarrow \infty$ here.

Energy E can be presented in the form:

$$E = b \frac{N}{r_0^6} (N - N_-)(N - N_+), \quad (11)$$

$$N_{\pm} = \frac{c r_0^5}{2b} \left[1 \pm \sqrt{1 - \frac{4ab}{c^2 r_0^6}} \right] > 0. \quad (12)$$

In the bound state, it should be $-\infty < E < 0$ what leads to condition $N_- < N < N_+$. Evaluating N as geometric mean $\sqrt{N_- N_+}$, we obtain that $N \propto r_0^2$.

Now we can estimate the central density:

$$\rho_0 \propto \frac{N}{r_0^3} \propto r_0^{-1}. \quad (13)$$

This dependence with $\beta = 1$ is obtained through a series of rough approximations and does not claim to be a final answer. However, the estimation obtained here is encouraging and stimulates us to study the model with potential ψ^6 .

B. “Core+Tail” Profile

Since the ψ^6 -model actually takes into account the three-particle interaction that is relevant under certain conditions in a small region of space (like a core), finding the distribution of dark matter in a large region of space requires an extension of the model. To extend this, we borrow ideas already applied to other models.

The large-scale structure simulation within the ψ DM model shows that there are structures (like filaments and voids) which are similar to the CDM outcomes. At the same time, DM distribution on a smaller, galactic scales differs due to the wave nature of ψ DM. Its prominent feature is formation of the coherent standing waves of

DM that form a flat core in the center of galactic DM halo. Such cores are described very well by the soliton-like solution of Schrödinger–Poisson equation also known as *boson star solution*. These cores are also surrounded by an envelope of incoherent phase, that mimics Navarro–Frenk–White (NFW) profile [8, 50].

Therefore, ψ DM profile is often represented as

$$\rho(r) = \rho_{core}(r) \theta(r_a - r) + \rho_{NFW}(r) \theta(r - r_a), \quad (14)$$

where $\theta(r)$ is a Heaviside theta-function. At the point $r = r_a$, we require $\rho_{core}(r_a) = \rho_{NFW}(r_a)$. Value of r_a is selected, for instance, to relate the mass of central soliton to the mass of whole DM halo as

$$M_s \propto M_{halo}^{1/3}. \quad (15)$$

This relation occurs in [34, 50] and reflects also equality of the energy per unit mass for the central core and the NFW envelope [32].

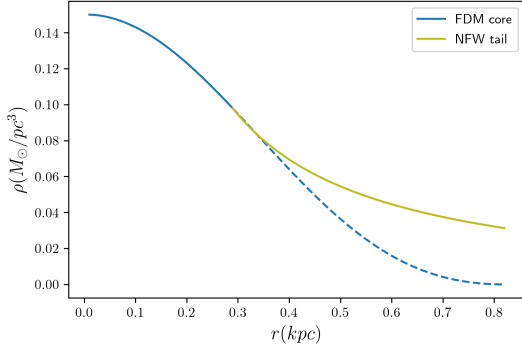


FIG. 1: The numerical FDM core solution with the NFW outer part.

A particular “extension” (14) of the FDM model, which is described by

$$-\Delta_r \psi(r) + \kappa U_{gr}(r) \psi(r) = \tilde{\gamma} \psi(r), \quad (16)$$

$$U_{gr}(r) = -\frac{1}{r} \int_0^r \psi^2(s) s^2 ds - \int_r^\infty \psi^2(s) s ds, \quad (17)$$

is sketched in Fig. 1 for central density $\rho_0 = 0.15 M_\odot \text{pc}^{-3}$ and particle mass $m = 1.6 \cdot 10^{-23} \text{ eV } c^{-2}$;

$$\kappa = \frac{8\pi G}{\hbar^2} \rho_0 m^2 r_*^4 \simeq 1.106; \quad r_* = 1 \text{ kpc}. \quad (18)$$

We would like to prove that a form (14) of DM profile, consisting of both soliton-like solution to the field equations in the inner region and NFW tail in the outer region of halo, remains correct for the self-interacting field. It is justified by evaluating the contribution of each term to the total energy. The same can be done by considering a ratio of these terms in the Schrödinger–Poisson equations.

Let us consider the decay rate $g(r)$ for the self-interaction \mathcal{E}_{int} with respect to the gravitational term \mathcal{E}_{gr} , which are given by (4). Thus, we introduce

$$g(r) = \frac{q(r)}{q(0)}, \quad q(r) = \frac{\mathcal{E}_{int}(r)}{\mathcal{E}_{gr}(r)}. \quad (19)$$

Evaluating $g(r)$, we use (6) again and obtain

$$g(r) = \frac{V_{gr}(0)}{V_{gr}(r)} e^{-4\frac{r}{r_0}} \simeq \frac{r}{r_0} e^{-4\frac{r}{r_0}}, \quad r > r_0. \quad (20)$$

On the other hand, there is the inner region $r < r_s$ with $g(r) \sim 1$, where r_s is some characteristic radius. This region should contain rather 1/4 of total halo mass like in a noninteracting field model.

Since $g(1.2r_0) \approx 0.01$ and $g(1.9r_0) \approx 0.001$, self-interaction can be neglected with a high accuracy in the outer region of halo. At the same time, the NFW approximation remains valid for the outer part of halo even in the case of a self-interacting field.

III. THE CASE OF TOMAS–FERMI APPROXIMATION

Although the distribution (14) is promising from the point of view of observations, a ψ^6 -model and its properties are of independent interest. In fact, we intend to study the boson subsystem formed by gravity and three-particle interaction, which can prevail at a high particle density in a small region of space like a galactic core.

Let us start from a macroscopic model of gravitating Bose–Einstein condensate with three-particle interaction, limiting ourselves by the spherically symmetric case and by the absence of hydrodynamic flows.

Introducing a constant chemical potential $\tilde{\mu}$, we will describe the condensate by real function $\psi(r)$ of radial variable $r = |\mathbf{r}|$. Thus, a starting point of our study is the energy functional in a ball $B = \{\mathbf{r} \in \mathbb{R}^3 | |\mathbf{r}| \leq R\}$:

$$\Gamma = 4\pi \int_0^R \left[\frac{\hbar^2}{2m} (\partial_r \psi(r))^2 + m \psi^2(r) V_{ext}(r) + \frac{U}{3} \psi^6(r) - \tilde{\mu} \psi(r)^2 \right] r^2 dr; \quad (21)$$

$$\Delta_r V_{ext}(r) = 4\pi G m |\psi(r)|^2, \quad (22)$$

where Δ_r is the radial part of Laplace operator (9).

For the sake of simplicity, let us introduce dimensionless variables:

$$\psi(r) = \sqrt{\varrho_0} \chi(\xi), \quad r = r_0 \xi, \\ A = 4\pi \frac{G m^3 \varrho_0 r_0^4}{\hbar^2}, \quad B = U \frac{\varrho_0^2 r_0^2 m}{\hbar^2}, \quad u = \tilde{\mu} \frac{m r_0^2}{\hbar^2}, \quad (23)$$

where $\chi(\xi)$ is a real dimensionless field; ϱ_0 and r_0 characterize *typical measures* of the central particle density and the system size, respectively.

Thus, we arrive at

$$\frac{\Gamma}{\Gamma_0} = \int_0^{\xi_B} \left[\frac{1}{2} (\partial_\xi \chi)^2 - u \chi^2 + A \chi^2 \varphi + \frac{B}{3} \chi^6 \right] \xi^2 d\xi, \\ \Gamma_0 = \frac{4\pi \hbar^2 r_0 \varrho_0}{m}, \quad \Delta_\xi \varphi(\xi) = \chi^2(\xi), \quad (24)$$

where $R = r_0 \xi_B$; Δ_ξ and Δ_ξ^{-1} are given by (9), (10) in terms of ξ replacing r ; also, $\chi(\xi) = \psi(r)/\sqrt{\varrho_0}$, see (23).

It is useful to evaluate immediately the range of model parameters. Turning to the known data for galactic cores, we assume that the central mass density $\rho_0 = m \varrho_0$ is of the order of magnitude $10^{-20} \text{ kg m}^{-3}$ and the light-boson mass m is of the order of $10^{-22} \text{ eV } c^{-2}$. Further, we use a definition of parameter A to determine the characteristic radius r_0 , defining a total radius $R = r_0 \xi_B$. One obtains

$$r_0 \simeq 0.824 \text{ kpc} \left[\frac{A}{10} \right]^{1/4} \left[\frac{mc^2}{10^{-22} \text{ eV}} \right]^{-1/2} \\ \times \left[\frac{\rho_0}{10^{-20} \text{ kg m}^{-3}} \right]^{-1/4}. \quad (25)$$

Since the realistic values of r_0 are smaller than 1 kpc, we estimate the measure of gravitational interaction as $A \sim 10$. Note that (25) cannot be regarded as relation between r_0 and ρ_0 discussed in the previous Section.

While the gravity looks like a cumulative effect of a whole system, (thermo)dynamics of internal processes is strongly determined by repulsive interaction among bosons, represented by parameter $B > A$.

The characteristic energy density is $\varepsilon_0 = \hbar^2 \varrho_0 / (m r_0^2)$. Combining this formula with (25), one gets

$$\varepsilon_0 \simeq 33.82 \text{ eV cm}^{-3} \left[\frac{A}{10} \right]^{-1/2} \left[\frac{mc^2}{10^{-22} \text{ eV}} \right]^{-1} \\ \times \left[\frac{\rho_0}{10^{-20} \text{ kg m}^{-3}} \right]^{3/2}. \quad (26)$$

In the pressure units, $33.82 \text{ eV cm}^{-3} \simeq 5.42 \cdot 10^{-12} \text{ Pa}$.

A detailed analysis of the model based on Γ will be performed in the next Section. However, before exploring the model in most general situation and in order to get an idea of the basic properties of the model, we first turn to the Thomas–Fermi approximation (at $\hbar \rightarrow 0$):

$$\frac{\Gamma_{\text{TF}}}{\Gamma_0} = \int_0^{\xi_B} \left[-u \eta + A \eta \varphi + \frac{B}{3} \eta^3 \right] \xi^2 d\xi, \quad (27)$$

where $\eta(\xi) = \chi^2(\xi)$ determines a local particle density.

The particle distribution $\eta(\xi)$ is found by extremizing functional Γ_{TF} , $\delta \Gamma_{\text{TF}} / \delta \eta(\xi) = 0$, that gives us an integral equation:

$$B \eta^2(\xi) + A \varphi(\xi) - u = 0, \quad \varphi(\xi) = \Delta_\xi^{-1} \eta(\xi). \quad (28)$$

We are interested in a solution which satisfies the following conditions:

$$\eta(0) = \eta_0, \quad \eta'(0) = 0, \quad \eta(\xi_B) = 0. \quad (29)$$

A chemical potential $\mu(\xi)$ of the system in gravitational field [52] is such that

$$\mu(\xi) + A \varphi(\xi) = u, \quad (30)$$

which is needed for further purposes. Taking (28) into account, $\mu(\xi)$ determines a particle density $\eta(\xi)$ as

$$\mu(\xi) = B \eta^2(\xi), \quad \mu(\xi_B) = 0. \quad (31)$$

Combining, $\mu(\xi)$ satisfies an equation:

$$\Delta_\xi \mu = -\frac{A}{\sqrt{B}} \mu^{1/2}, \quad \mu(0) = B \eta_0^2, \quad \mu'(0) = 0. \quad (32)$$

To compute η (and μ), we first transform $\varphi(\xi)$ as

$$\varphi(\xi) = -\frac{1}{\xi} \int_0^\xi \eta(s) s^2 ds - \int_\xi^{\xi_B} \eta(s) s ds \\ = -v(\xi_B) + \frac{1}{\xi} \int_0^\xi v(s) ds, \quad (33)$$

where an auxiliary field $v(\xi)$ is defined by

$$\partial_\xi v(\xi) = \xi \eta(\xi), \quad v(0) = 0; \quad v(\xi) = \int_0^\xi \eta(s) s ds. \quad (34)$$

Thus, Eq. (32) is solved at $\mu(0) = \nu$, where new parameter

$$\nu = A v(\xi_B) + u > 0 \quad (35)$$

absorbs unknown $v(\xi_B)$ due to arbitrariness of $u < 0$.

Transformation (33) allows us to rewrite Γ_{TF} in alternative form:

$$\frac{\Gamma_{\text{TF}}}{\Gamma_0} = \int_0^{\xi_B} \left[-u \eta(\xi) + \frac{B}{3} \eta^3(\xi) \right] \xi^2 d\xi \\ - \frac{A}{2} \int_0^{\xi_B} [v(\xi_B) - v(\xi)]^2 d\xi. \quad (36)$$

Here, the contributions of repulsive and attractive interactions are easily recognized.

To obtain (28) by varying (36) with respect to η , we should take the relations (34) into account. Thus, using our notations, (28) can be reduced to the set of equations:

$$\partial_\xi v(\xi) = \xi \eta(\xi), \quad v(0) = 0, \quad (37)$$

$$\eta(\xi) = \sqrt{\eta_0^2 - \frac{k}{\xi} \int_0^\xi v(s) ds}, \quad \eta_0 = \sqrt{\frac{\nu}{B}}, \quad (38)$$

where parameters η_0 and $k = A/B$ should be given. Equation (38) indicates that function $\eta(\xi)$ vanishes at some $\xi = \xi_B$, depended on the parameters used (see Fig. 2, dashed curves).

In a consistent way, we get at the boundary $\xi = \xi_B$:

$$\frac{A}{\xi_B} \int_0^{\xi_B} v(\xi) d\xi = \nu, \quad u = -\frac{A}{\xi_B} \int_0^{\xi_B} \eta(\xi) \xi^2 d\xi. \quad (39)$$

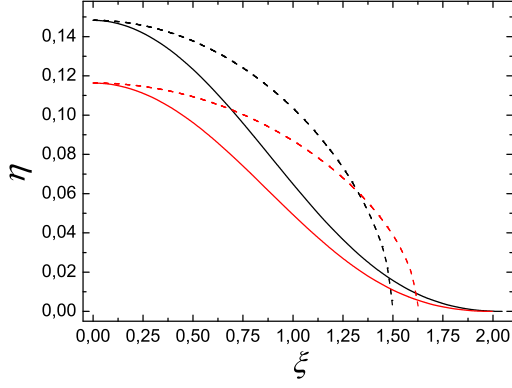


FIG. 2: Spatial development of particle density $\eta(\xi) = \chi^2(\xi)$ in the models with both quantum fluctuations (solid) and in TF approximation (dashed) at $A = 10$ and the same initial condition. Black and red curves correspond to $B = 20$ and $B = 30$, respectively. For solid curves see the text after Eq.(60) below.

Therefore, a negative chemical potential u coincides with the (dimensionless) gravitational potential of a whole system at the boundary.

We solve numerically the set of equations (38), using the Euler's method, to find fields $\eta(\xi)$ and $v(\xi)$. It is because this set is not integrable analytically.

Particularly, at $A = B = \nu$, what can be achieved by rescaling, the problem coincides with the Lane–Emden equation with polytropic index $p = 1/2$ for $\theta(\xi) = \eta^2(\xi)$ (see (32)):

$$\Delta_\xi \theta(\xi) = -\theta^p(\xi), \quad \theta(0) = 1. \quad (40)$$

Note that it has $\xi_B^{exact} \simeq 2.75269805$ [51].

In general case, we are interested in looking for macroscopic characteristics of the system like an extreme Γ_{TF}^{ex} , obtained from Γ_{TF} by inserting the solution $\eta(\xi)$.

Technically, varying A , B and ν , functions $\eta(\xi)$ and $v(\xi)$ (together with the values of ξ_B and $v(\xi_B)$) can be found (numerically) in accordance with (37) and (38). Using the relation $u = \nu - A v(\xi_B)$ and (36), we are able to compute Γ_{TF}^{ex} and the others.

Finding macroscopic characteristics, we appeal to the thermodynamic relations at $T = 0$:

$$dp(\xi) = \eta(\xi) d\mu(\xi), \quad p(\xi_B) = 0, \quad (41)$$

$$\varepsilon(\xi) = \eta(\xi) \mu(\xi) - p(\xi), \quad \varepsilon(\xi_B) = 0, \quad (42)$$

where functions $p(\xi)$ and $\varepsilon(\xi)$ determine the (dimensionless) mean pressure P and the internal energy E :

$$P = \frac{3}{\xi_B^3} \int_0^{\xi_B} p(\xi) \xi^2 d\xi, \quad E = \int_0^{\xi_B} \varepsilon(\xi) \xi^2 d\xi. \quad (43)$$

Hereafter, $\xi_B^3/3$ represents the volume of the system.

Therefore, we need to integrate first the Gibbs–Duhem relation (41) and to substitute $p(\xi)$ into the Euler relation

(42) in order to find $\varepsilon(\xi)$. Thus, one obtains the explicit expressions:

$$p(\xi) = \frac{2}{3} B \eta^3(\xi), \quad \varepsilon(\xi) = \frac{1}{3} B \eta^3(\xi), \quad (44)$$

which give us the equation of state by inserting the solution $\eta(\xi)$ of (37)–(38).

It is instructive to express the *gravitational energy* E_{gr} ,

$$E_{gr} = \frac{A}{2} \int_0^{\xi_B} \eta(\xi) \varphi(\xi) \xi^2 d\xi, \quad (45)$$

the *internal energy* E and the *total energy* $E_{tot} = E + E_{gr}$ in terms of gravitational potential u at the boundary:

$$u\mathcal{N} = -A \frac{\mathcal{N}^2}{\xi_B}, \quad \mathcal{N} = \int_0^{\xi_B} \eta(\xi) \xi^2 d\xi. \quad (46)$$

Using the auxiliary notations and formulas:

$$n(\xi) = \int_0^\xi \eta(s) s^2 ds, \quad \mathcal{N} = n(\xi_B), \quad (47)$$

$$\varphi(\xi) = -\frac{\mathcal{N}}{\xi_B} - \int_\xi^{\xi_B} \frac{n(s)}{s^2} ds, \quad (48)$$

$$\partial_\xi \left(\frac{n^2(\xi)}{\xi} \right) + \frac{n^2(\xi)}{\xi^2} = 2 \frac{n(\xi)}{\xi} \frac{\partial_\xi n(\xi)}{\xi}, \quad (49)$$

$$\frac{1}{\eta(\xi)} \partial_\xi p(\xi) = \partial_\xi \mu(\xi) = -A \frac{n(\xi)}{\xi^2}, \quad (50)$$

one obtains

$$\int_0^{\xi_B} p(\xi) \xi^2 d\xi = \frac{2A}{9} \frac{\mathcal{N}^2}{\xi_B}, \quad E_{gr} = -\frac{2A}{3} \frac{\mathcal{N}^2}{\xi_B}, \quad (51)$$

$$E = \frac{A}{9} \frac{\mathcal{N}^2}{\xi_B}, \quad E_{tot} = -\frac{5A}{9} \frac{\mathcal{N}^2}{\xi_B}, \quad (52)$$

which agree with the general results [52] for gravitating systems with polytropic equation of state at $T = 0$.

IV. THE PROCESSES DRIVEN BY QUANTUM FLUCTUATIONS

Let us return to the model with the included quantum kinematics, which is initially described by functional (24). The field equations read

$$\frac{1}{2} \Delta_\xi \chi + u\chi - A\chi\varphi - B\chi^5 = 0, \quad \Delta_\xi \varphi = \chi^2. \quad (53)$$

We combine the model equations in the spirit of the previous Section by introducing field $v(\xi)$. It gives us

$$\begin{aligned} 2 \frac{\Gamma}{\Gamma_0} = \int_0^{\xi_B} \left[(\partial_\xi \chi)^2 - u_* \chi^2(\xi) + \frac{B_*}{3} \chi^6(\xi) \right] \xi^2 d\xi \\ - \frac{A_*}{2} \int_0^{\xi_B} [v(\xi_B) - v(\xi)]^2 d\xi, \end{aligned} \quad (54)$$

$$\Delta_\xi \chi + \nu\chi - \chi \frac{A_*}{\xi} \int_0^\xi v(s) ds - B_* \chi^5 = 0, \quad (55)$$

$$\partial_\xi v(\xi) = \xi \chi^2(\xi), \quad v(0) = 0, \quad (56)$$

$$\nu = A_* v(\xi_B) + u_*, \quad (57)$$

where $A_* = 2A$, $B_* = 2B$ and ν (instead of $u_* = 2u$) are arbitrary positive parameters. The system boundary ξ_B is defined from condition $\chi(\xi_B) = 0$ and is the *first zero* of oscillating function $\chi(\xi)$. Of course, the values of ξ_B would differ from those in the TF approximation at the same A and B that can be seen in Fig. 2.

Aiming to obtain a solution with a finite initial value $\chi_0 = \chi(0) < \infty$, it is naturally to require $\chi'(0) = 0$. In order to obtain a decaying solution (finite for admissible ξ), we formulate the following conditions which fix χ_0 .

Expanding $\chi(\xi) = \chi_0 + C_2\xi^2 + \dots$ at $\xi \rightarrow 0$ and substituting it in (55), (56), the set of algebraic equations arises:

$$\begin{aligned} 6C_2 + \nu\chi_0 - B_*\chi_0^5 &= 0, \\ \nu C_2 - \frac{A_*}{6}\chi_0^3 - 5B_*\chi_0^4 C_2 &= 0. \end{aligned} \quad (58)$$

Combining, the initial value χ_0 should satisfy the equation $S(A_*, B_*, \nu, \chi_0) = 0$, where

$$S(A_*, B_*, \nu, z) = A_*z^2 - (5B_*z^4 - \nu)(\nu - B_*z^4), \quad (59)$$

together with condition $2C_2 = \chi''(0) \leq 0$. These constraints limit χ_0 as $(\nu/5B_*)^{1/4} < \chi_0 < (\nu/B_*)^{1/4}$.

In practice, three regimes (for given A_* , B_* and ν) are observed: 1) no solution; 2) single solution; 3) pair of (positive) solutions. Usually, for fixed A_* and B_* , but increasing ν , the indicated sequence of all three modes occurs.

The absence of a solution of (58) in step 1) leads to the only possible solution to the autonomous equation (55): $\chi(\xi) = 0$. At the stage 2), we obtain a *minimal admissible value* ν_{\min} . Starting from this threshold, the system begins to evolve. At the stage 3), one of the values of χ_0 , which corresponds to a minimal of these, should be chosen (because the other leads to divergent $\chi(\xi)$).

Actually, all quantities of the model, computed at fixed A and B , are supposed to be functions of free parameter ν . Thus, dependence, say, of a on b should be treated in parametric form: $a(b) = \{(b(\nu), a(\nu)) | \nu \geq \nu_{\min}\}$.

The possible dependencies of χ_0 on ν are shown in Fig. 3 (a). We present also the values of ξ_B in Fig. 3 (b), which are used in order to limit the system size. Particular distributions of particles at $\xi \leq \xi_B$ can be seen in Fig. 2 (solid lines).

Fig. 3 reveals two different modes of model behavior, which are separated by a turning point. We assume that the change of regime is associated with a *phase transition*, which we will study. Moreover, the system size in Fig. 3 (b) does not depend completely on parameters A and B of interactions (in contrast to [22]), but is affected also by ν which defines the dominant phase of matter.

For a deeper understanding of the model properties, let us define a chemical potential $\mu_q(\xi)$ as

$$\mu_q(\xi) + A\varphi(\xi) - \frac{1}{2\chi(\xi)}\Delta\xi\chi(\xi) = u. \quad (60)$$

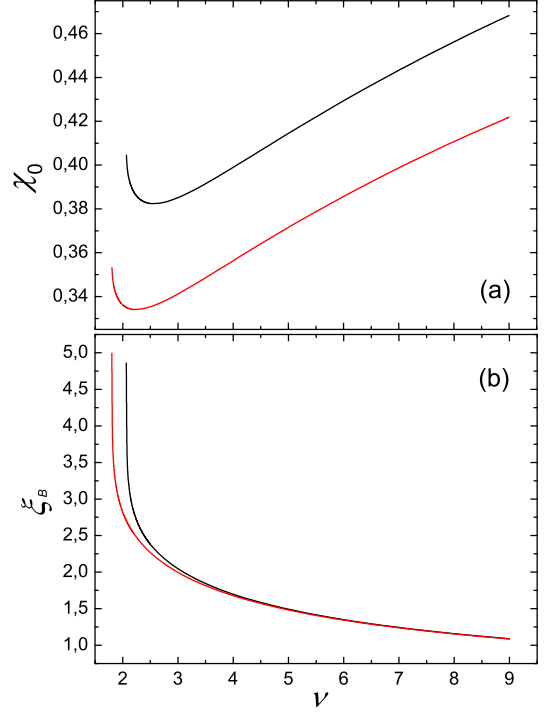


FIG. 3: Characteristics of $\chi(\xi)$ versus parameter ν at $A = 10$. Black and red lines correspond to $B = 20$ and $B = 30$, respectively. Panel (a) represents the initial values χ_0 determined from (58). Panel (b) shows the values of first zero, when $\chi(\xi_B) = 0$. These are built at $\nu_{\min}^{\text{black}} \simeq 2.066$ and $\nu_{\min}^{\text{red}} \simeq 1.805$ found numerically.

Accordingly to the equation of motion (53), μ_q determines χ as

$$\mu_q(\xi) = B\chi^4(\xi), \quad \mu_q(\xi_B) = 0. \quad (61)$$

Replacing μ with μ_q in (41)–(42), we reproduce the expressions (44) for the internal energy density $\varepsilon(\xi)$ and the local pressure $p(\xi)$ at $\eta = \chi^2$.

Internal pressure $p(\xi)$ evolves spatially as

$$\frac{\partial_\xi p(\xi)}{\eta(\xi)} = \partial_\xi \mu_q(\xi) = -A \frac{n(\xi)}{\xi^2} + \partial_\xi \left(\frac{1}{2\chi(\xi)} \Delta\xi\chi(\xi) \right), \quad (62)$$

what is in contrast with (50) in the TF approximation. This is a complicated hydrostatic equation (similar to Eq. (15) in [53]), and we do not find its solution. Moreover, all necessary fields can be found directly on the base of (55)–(57).

Nevertheless, (62) says that internal pressure p is balanced by the resulting pressure caused by gravity and quantum fluctuations. It is interesting to evaluate the contributions of these effects.

To do this, we turn to more simple and known relations:

$$p = \frac{2}{3}B\chi^6 = \frac{2}{3} \left[\frac{1}{2}\chi\Delta\xi\chi + u\chi^2 - A\chi^2\varphi \right], \quad (63)$$

where (53) is inserted.

Since the chemical potential u consists here of two parts, accordingly to (57), we introduce the following components of pressure:

$$p_\nu = \frac{1}{3} (\chi \Delta_\xi \chi + \nu \chi^2), \quad (64)$$

$$p_{\text{gr}} = -\frac{2}{3} A \eta [v(\xi_B) + \varphi(\xi)], \quad (65)$$

which give us $p_\nu + p_{\text{gr}} = p$ by construction. We can see that $p_\nu \sim \chi^2$ and corresponds to the wave fluctuations, regulated by free parameter ν , while $p_{\text{gr}} \sim \chi^4$ and describes pair interaction which is controlled by gravitational constant G absorbed by parameter A .

Average value of pressure p_{gr} is given by expression:

$$V P_{\text{gr}} = -\frac{2}{3} A \int_0^{\xi_B} v(\xi) [v(\xi_B) - v(\xi)] d\xi < 0. \quad (66)$$

This means that the pressure created by interactions is $P - P_{\text{gr}} > 0$. At the same time, $P_\nu > 0$ supports the pressure inside the system. From another point of view, action of P_ν (mean value of p_ν) is equivalent to external influence on the system.

Let us show how p_ν can be related with an external field h of Landau theory [52]. First of all, we assume that the unperturbed theory is given by Γ_{TF} . Associating a perturbation with including quantum fluctuations and field ν , given by hands, a perturbation part of a total functional Γ is presented in the form:

$$2 \frac{\Gamma_{\text{pert}}}{\Gamma_0} = - \int_0^{\xi_B} \eta(\xi) h(\xi) \xi^2 d\xi, \quad (67)$$

$$h(\xi) = \frac{1}{\chi(\xi)} \Delta_\xi \chi(\xi) + \nu. \quad (68)$$

Therefore, the equation of motion here reads $(\delta\Gamma/\delta\eta(\xi))_{h=\text{const}} = 0$, what leads to (53). It immediately means also that the particle density $\eta(\xi)$ is an order parameter (conjugated to h) of such a theory. To assign a physical meaning to this perturbation, we see a product $\eta(\xi)h(\xi)$ is nothing but the pressure p_ν .

Often phase transitions are associated with changes of intensive parameters like temperature and pressure (in the absence of magnetic and electric fields). Since $T = 0$ in our model, changes are stimulated by pressure. Microscopically, our assumption of a phase transition in the model can now be justified by the presence of a perturbation P_ν related to quantum fluctuations as well as the form of interaction that allows the existence of two nonequivalent phases of matter.

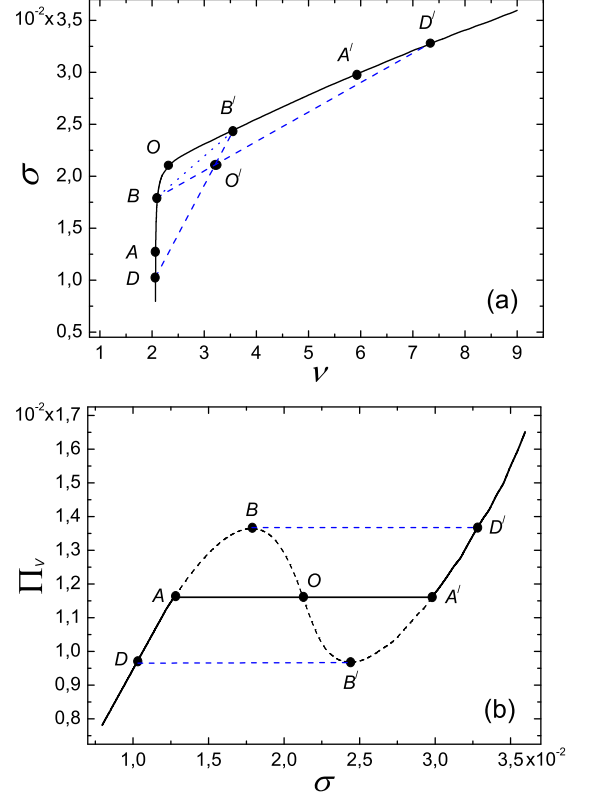


FIG. 4: Discontinuity of mean density σ at fixed $A = 10$, $B = 20$ and at varying ν (a) and Π_ν (b). Panel (b) shows the metastable (AB and $A'B'$) and unstable (BB') states. Straight line AA' is constructed by the Maxwell rule. The connections between key points in Panel (b) are *schematically* transferred to Panel (a).

V. THERMODYNAMICAL QUANTITIES AND TWO PHASES OF DARK MATTER

To analyze the macroscopic properties of the model, we use a set of dimensionless quantities:

$$P = \frac{2B}{\xi_B^3} \int_0^{\xi_B} \chi^6(\xi) \xi^2 d\xi, \quad (69)$$

$$\Pi_\nu = -\frac{(B/A)}{\xi_B^3} \int_0^{\xi_B} [(\partial_\xi \chi(\xi))^2 - \nu \chi^2(\xi)] \xi^2 d\xi, \quad (70)$$

$$\sigma = \frac{3}{\xi_B^3} \int_0^{\xi_B} \chi^2(\xi) \xi^2 d\xi, \quad (71)$$

$$\tau = \frac{3}{\xi_B^3} \int_0^{\xi_B} (\partial_\xi \chi(\xi))^2 \xi^2 d\xi, \quad (72)$$

which are obtained by averaging over volume $V = \xi_B^3/3$ of $p(\xi)$ (internal pressure), $(B/A)p_\nu(\xi)$ (perturbation pressure rescaled for convenience), $\eta(\xi) = \chi^2(\xi)$ (particle density), and $-\chi(\xi)\Delta_\xi \chi(\xi)$ (measure of fluctuations), respectively. Since the functions of our interest are depended on ν , χ_0 and ξ_B , we also pay attention to their behavior. We omit consideration of the quantities as-

sociated with the already given, such as internal energy $E = VP/2$.

To convert the dimensionless quantities τ , ε , p , P and Π_ν into physical units, we should multiply these by ε_0 from (26). The value of mean mass density is $\rho_0\sigma$.

Before a detailed description of the processes in the system, we want to check the hypothesis of a phase transition. Since the only characteristic of matter here is its density σ , let us trace its changes under different (external) factors like ν and Π_ν . Results of numerical calculations are presented in Fig. 4. Note immediately that the dependence of σ on measure of fluctuations τ (given by graphic $\sigma(\tau) = \{(\tau(\nu), \sigma(\nu)) | \nu \geq \nu_{\min}\}$) looks similar to Fig. 4 (a) and, thus, is omitted here.

First of all, we note a steep change of $\sigma(\nu)$ in Fig. 4 (a) at $\nu_{\min} \simeq 2.066$. As was argued above, $\chi(\xi) = 0$ and, as a result, $\sigma = 0$ at $\nu < \nu_{\min}$, while $\sigma(\nu_{\min}) > 0$. It can be interpreted as a first-order phase transition. This phenomenon appears due to the rule of finding initial condition χ_0 (58). However, this is not the subject of our study. More interesting for us is a behavior of the matter near a turning point O , that is, at $\nu \rightarrow \nu_{\min}$.

To understand the processes near the point O , we appeal to Fig. 4 (b). Indeed, backbending in Fig. 4 (b) reveals the first-order phase transition, which exhibits existence of “gaseous” and “liquidlike” phases of the matter. This process differs from the familiar boiling water due to our consideration of the quantum system at $T = 0$ and the mechanism which is based on quantum fluctuations or, alternatively, associated with compression Π_ν (that may be convenient further when considering variations in macroscopic parameters).

The characteristics, computed numerically, are depicted in Fig. 5 and behave as multivalued functions of Π_ν . These graphics represent isotherms at $T = 0$. Varying the parameter B (and A), we can conclude that the region of backbending presence, projected onto Π_ν axis, remains the same due to scale factor B/A , appeared by defining Π_ν . It means that there is no possibility to achieve the critical point of phase transition, when $\partial\Pi_\nu/\partial f = 0$ and $\partial^2\Pi_\nu/\partial f^2 = 0$ simultaneously for any f of these functions, by changing B (and A). Comparing with water, in this model there is no natural parameter analogous to temperature, the increase of which would lead to boiling. We admit that by considering $T > 0$, one cannot also observe a similar process, because a vaporization temperature here is expected to be much higher than the critical temperature of the condensate and to be comparable (in the energy units) with the gravitational energy of the system. Nevertheless, Fig. 5 allows us to extract the conditions of transition between gaseous and liquid-like phases at $T = 0$, if such a situation is realized in nature.

Considering Π_ν as external compression for convenience and omitting a physical interpretation of the region of instability (like BB' in Fig. 4), Fig. 5 permits to conclude the following. By intensifying the compression Π_ν , starting from the minimum, we can see the size ξ_B

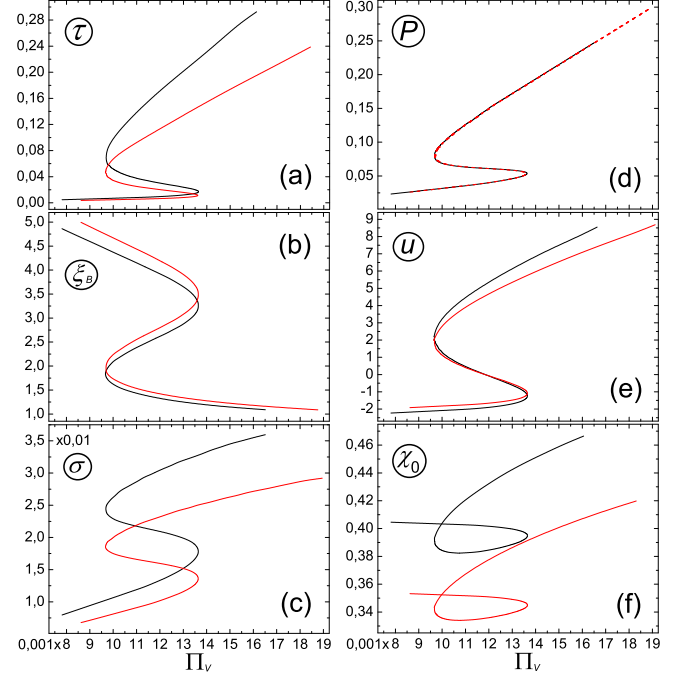


FIG. 5: Dependence of dimensionless characteristics on Π_ν at $A = 10$. Black and red lines correspond to $B = 20$ and $B = 30$, respectively.

(b) of the system decreases, and the mean density σ (c) increases throughout the process. At the same time, the central density χ_0^2 (see (f)) and fluctuations τ (a) do not noticeably change at the first stage, but begin to grow significantly after the transition to a more dense, liquid-like phase. A similar behavior is observed for chemical potential u (e) and internal pressure P (see (d), where curves with different B overlap). As it could be expected the point of two phases coexistence, $u = 0$, lies in the instability region.

Note that in all the figures wherein the dependence on compression Π_ν is involved, we observe the common feature — existence of the same pair of special/distinguished values of Π_ν , that is $\Pi_\nu^{(1)} \simeq 9.65 \cdot 10^{-3}$ and $\Pi_\nu^{(2)} \simeq 13.65 \cdot 10^{-3}$ in dimensionless units (or, in physical units, $\Pi_\nu^{(1)} \simeq 5.23 \cdot 10^{-14}$ Pa and $\Pi_\nu^{(2)} \simeq 7.40 \cdot 10^{-14}$ Pa). Due to that, the curves are separated in three regions of qualitatively differing behavior: two “normal” parts filled with stable states of the system, which correspond to compressions such that $\Pi_\nu \leq \Pi_\nu^{(1)}$ and $\Pi_\nu \geq \Pi_\nu^{(2)}$ respectively, and the interval/region of instability. As seen from the figures, for the latter interval there appears an obvious backbending which shows the opposite behavior of the considered functions as compared to the normal (stable) parts of the curves.

Our results predict significant fluctuations τ in the denser state of dark matter. Physically, this is due to the increasing role of repulsion χ^6 among particles by growing σ . Although, associating τ with the effective temperature, the liquidlike phase of DM can be assumed to be

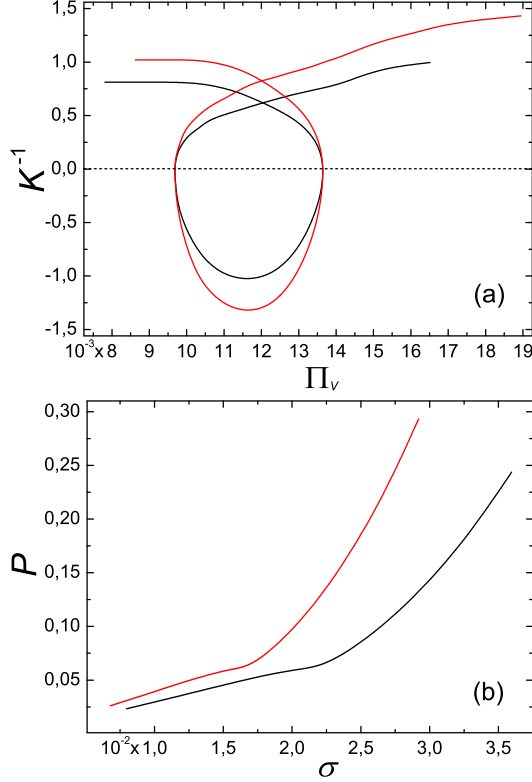


FIG. 6: Behavior of incompressibility K^{-1} and internal pressure P at $A = 10$. Black and red lines correspond to $B = 20$ and $B = 30$, respectively.

in thermalized state what is already noted in [54] within the SIDM model. A simultaneous increase in “temperature” τ and density σ resembles the behavior of water in the temperature range $t = 0 \div 4^\circ\text{C}$.

Isothermal compressibility K , playing the role of susceptibility, and its inverse K^{-1} defined here as

$$K = \frac{\partial \sigma}{\partial \Pi_\nu}, \quad K^{-1} = \frac{\partial \Pi_\nu}{\partial \sigma}, \quad (73)$$

are also important characteristics and can be computed numerically (with high precision loss) by using dependencies in Fig. 5 (c). The result is sketched in Fig. 6 (a).

The most important positive (or regular) part, with $K^{-1} > 0$, consists of two branches which describe the two distinct phases of matter with their individual properties. It is interesting to remark that the incompressibility behaves like a constant for lower values of compression, say for $\Pi_\nu \leq \Pi_\nu^{(1)}$, whereas it shows rising property for higher values when Π_ν grows, including the region with $\Pi_\nu > \Pi_\nu^{(2)}$.

On the other hand, there is a negative part of incompressibility, $K^{-1} < 0$, that means the instability region, which corresponds to the intermediate values of compression, i.e. for $\Pi_\nu^{(1)} < \Pi_\nu < \Pi_\nu^{(2)}$. Using equilibrium statistics, this is usually neglected in the physical picture. However, as shown in some papers, there exist in reality the structures (materials) characterized by negative K ,

see e.g. [55–58]. Besides, as some works demonstrate, the vanishing value of the effective speed of sound (that would happen in our model at $\Pi_\nu = \Pi_\nu^{(1)}$ and $\Pi_\nu = \Pi_\nu^{(2)}$), may be also of importance [59, 60]. Therefore, the peculiar instability region, together with vanishing property in some points, may be taken into account more seriously in the context of the present model, and the physical meaning of all these unusual properties deserves more detailed study.

Dependence of internal pressure P (and internal energy E) on mean density σ in Fig. 6 (b) indicates rather a second-order phase transition with a turning point at $\partial^2 P / \partial \sigma^2 = 0$. Studying numerically the dependencies P on σ for different values of A and B , which are not shown here, the presence of a backbending (accompanying a first-order phase transition) was not confirmed.

Thus, the visualized equation of state also reveals two phases. However, it does not permit us to explain in details a mechanism of phase transition. Moreover, increasing a parameter B , the system jumps into liquid-like phase at smaller values of σ . This probably witnesses enhanced role of three-particle interaction.

There is one further feature of the role of parameter B (at fixed $A < B$) clearly seen from Figs. 2,3,5,6. Namely, its influence on the studied thermodynamical quantities is the following: the greater is (the value of) B the higher are the quantities $\xi_B(\Pi_\nu)$, $K^{-1}(\Pi_\nu)$ and $P(\sigma)$; on the contrary, regularity is inverse for the density $\eta(\xi)$, $\chi_0(\Pi_\nu)$, $\chi_0(\nu)$, $\xi_B(\nu)$, $\tau(\Pi_\nu)$, $u(\Pi_\nu)$ and $\sigma(\Pi_\nu)$. At last, there is a special case — the quantity $P(\Pi_\nu)$, see Fig. 5d, which shows (almost) no dependence on the value of B .

Adiabatic speed of sound c_s can be found (in physical units) as

$$c_s = \sqrt{\left. \frac{\varepsilon_0}{\rho_0} \frac{\partial p}{\partial \eta} \right|_{\eta=\chi_0^2}} = \frac{\hbar \sqrt{2B}}{m r_0} \chi_0^2. \quad (74)$$

Thus, the magnitude of c_s is evaluated as

$$c_s \simeq 2.36 \cdot 10^6 \text{ cm s}^{-1} \left[\frac{A}{10} \right]^{-1/4} \left[\frac{B}{20} \right]^{1/2} \left[\frac{\chi_0}{0.4} \right]^2 \times \left[\frac{m c^2}{10^{-22} \text{ eV}} \right]^{-1/2} \left[\frac{\rho_0}{10^{-20} \text{ kg m}^{-3}} \right]^{1/4}. \quad (75)$$

This value is in accordance with the predictions of other models [53].

VI. CONCLUDING REMARKS

The results obtained above witness clearly that the inclusion of sixth order repulsive self-interaction of ultralight dark matter within the particular modification of Gross–Pitaevskii equation leads to highly nontrivial properties of BEC DM and thus to unexpected galactic core structure and dynamics. The main results of the study, obtained numerically, are presented in the form of

Figs. 3–6, equipped with comments in the text, which we do not repeat here.

There is a principal issue of whether the BEC dark bosons are viewed as *elementary or composite*: the answer to this could give some guess towards revealing the nature of dark matter. If deformed bosons are dealt with, then (i) some additional interaction between bosons, besides the familiar pure bosonic attraction of quantum-statistical origin, can be effectively taken into account [61], also (ii) a rather simple effective account of compositeness aspects is as well at our disposal [62–64], and (iii) these two issues can be treated jointly [65–67]. It is important to emphasize that compositeness and the related deformation significantly affect [45, 68] the critical temperature of condensation, depending on the constituent particles so that the case of Bose-Bose composites basically differs from that of Fermi-Fermi composites.

As mentioned in the Introduction, the nontrivial phase structure of the core in the central part of DM halo was noticed in the work of Chavanis [17] (namely the existence of dilute and dense phases, and the related *zero's order* phase transition seen through the mass-radius relation). Unlike that, in the present work we have demonstrated both the presence of two phases (consisting of stable, metastable, and unstable branches) and of the *first-order* phase transition.

It was already pointed out that phase transitions in dark matter can trigger *gravitational waves* [69–71], see also [72]. Especially this can hold if one takes into account that the nontrivial phase structure can even more naturally occur when we deal with the colliding (or merger of) two galaxies, see e.g. [71, 73, 74]. In this context, it would be interesting to investigate possible

generation of gravitational waves caused by the phase transitions (in DM core) of the form described in this paper, possibly with extension of the model through inclusion of dynamical aspects. Till that will be performed, the results described above, in particular those visualized in Figs. 3–6, can be viewed as a “screen-shot” (or fixed-time slice) of the whole picture. The complete dynamics (continuous time evolution) is obviously needed, and separate work will be devoted to this subject.

No doubt of importance is the necessity to consistently study the simultaneous presence of both quartic and sextic terms in the scalar potential. If both these terms are repulsive, the inclusion of the 4th order term should somewhat enhance the effects of the sixth order self-interaction term studied above. Not less interesting and important task is to establish the exact nature (structure) of the appearing two distinct phases manifested by the DM core. To this end, the role of three-particle interactions should be studied within the quantum-mechanical framework. In this context, knowledge of the second and third virial coefficients of $\tilde{\mu}, q$ -deformed Bose gas model [67] could be helpful. We hope to report on such results elsewhere.

Acknowledgements

A.M.G. acknowledges support from the National Academy of Sciences of Ukraine by its priority project No. 0120U100935 “Fundamental properties of the matter in the relativistic collisions of nuclei and in the early Universe”. The work of A.V.N. was supported by the project No. 0117U000238 of the National Academy of Sciences of Ukraine.

-
- [1] F. Zwicky, *Astrophys. J.* **86**, 217 (1937).
 - [2] G. Bertone and D. Hooper, *Rev. Mod. Phys.* **90**, 045002 (2018).
 - [3] S.-J. Sin, *Phys. Rev. D* **50**, 3650 (1994).
 - [4] J.-W. Lee and I.-G. Koh, *Phys. Rev. D* **53**, 2236 (1996).
 - [5] W. Hu, R. Barkana, and A. Gruzinov, *Phys. Rev. Lett.* **85**, 1158 (2000).
 - [6] A. Suarez, V. Roblez, and T. Matos, *Astrophys. Space Sci. Proc.* **38**, 107 (2014).
 - [7] J.-W. Lee, *EPJ Web Conf.* **168**, 06005 (2018).
 - [8] L. Hui, J.P. Ostriker, S. Tremaine, and E. Witten, *Phys. Rev. D* **95**, 043541 (2017).
 - [9] L.A. Urena-Lopez, *EPJ Web Conf.* **168**, 06005 (2018).
 - [10] E.G.M. Ferreira, *Ultra-Light Dark Matter*, *astro-ph/2005.03254*.
 - [11] J.J. Fan, *Phys. Dark Univ.* **14**, 84 (2016).
 - [12] P.J.E. Peebles, *Astrophys. J. Lett.* **534**, L127 (2000).
 - [13] L. Berezhiani and J. Khoury, *Phys. Rev. D* **92**, 103510 (2015).
 - [14] J. Goodman, *New Astron.* **5**, 103 (2000).
 - [15] C.G. Bohmer and T. Harko, *J. Cosmol. Astropart. Phys.* **06**, 025 (2007).
 - [16] P.H. Chavanis, *Eur. Phys. J. Plus* **132**, 248 (2017).
 - [17] P.H. Chavanis, *Phys. Rev. D* **98**, 023009 (2018).
 - [18] V. Sahni and L. Wang, *Phys. Rev. D* **62**, 103517 (2000).
 - [19] T. Matos and L.A. Urena-Lopez, *Class. Quant. Grav.* **17**, L75 (2001).
 - [20] M. Alcubierre, F.S. Guzman, T. Matos, D. Nunez, L.A. Urena-Lopez, and P. Wiederhold, *Class. Quant. Grav.* **19**, 5017 (2002).
 - [21] G.R. Blumenthal, S.M. Faber, J.R. Primack, and M.J. Rees, *Nature* **311**, 517 (1984).
 - [22] T. Harko, *J. Cosmol. Astropart. Phys.* **05**, 022 (2011).
 - [23] H. Deng, M.P. Hertzberg, M.H. Namjoo, and A. Masoumi, *Phys. Rev. D* **98**, 023513 (2018).
 - [24] M.Yu. Khlopov, B.A. Malomed and Ya.B. Zeldovich, *Mon. Not. R. Astron. Soc.* **215**, 575, (1985).
 - [25] T. Harko, *Phys. Rev. D* **89**, 084040 (2014).
 - [26] P. Salucci, *Astron. Astrophys. Rev.* **27**, 2 (2019).
 - [27] A. Diez-Tejedor, A.X. Gonzalez-Morales, and S. Profumo, *Phys. Rev. D* **90**, 043517 (2014).
 - [28] X. Zhang *et al.*, *Eur. Phys. J. C* **78**, 346 (2018).
 - [29] E. Kun, Z. Keresztes, and L. Gergely, *Astron. Astrophys.* **633**, A75 (2020).
 - [30] M. Craciun and T. Harko, *Roman. Astron. J.* **29**, 109 (2019).

- [31] E. Castellanos, C. Escamilla-Rivera, *Int. J. Mod. Phys. D* **29**, 2050063 (2020).
- [32] N. Bar, D. Blas, K. Blum, and S. Sibiryakov, *Phys. Rev. D* **98**, 083027 (2018).
- [33] J.-W. Lee, *Phys. Lett. B* **756**, 166 (2016).
- [34] H.-Y. Schive, M.-H. Liao, T.-P. Woo, S.-K. Wong, T.-H. Chiueh, T. Broadhurst, and W.-Y. Pauchy Hwang, *Phys. Rev. Lett.* **113**, 261302 (2014).
- [35] P. Sikivie and Q. Yang, *Phys. Rev. Lett.* **103**, 111301 (2009).
- [36] T. Noumi, K. Saikawa, R. Sato, and M. Yamaguchi, *Phys. Rev. D* **89**, 065012 (2014).
- [37] S. Davidson, *Astropart. Phys.* **65**, 101 (2015).
- [38] A.H. Guth, M.P. Hertzberg, and C. Prescod-Weinstein, *Phys. Rev. D* **92**, 103513 (2015).
- [39] E.D. Schiappacasse and M.P. Hertzberg, *JCAP* **1801**, 037 (2018).
- [40] T.R. Govindarajan and N. Kalyanapuram, *Mod. Phys. Lett. A* **34**, 1950330 (2019).
- [41] S. Das and R.K. Bhaduri, *Class. Quant. Grav.* **32**, 105003 (2015).
- [42] E. Kun, Z. Keresztes, S. Das, and L.A. Gergely, *Symmetry* **10**, 520 (2018).
- [43] C. de Rham, J.T. Deskins, A.J. Tolley, and S.-Y. Zhou, *Rev. Mod. Phys.* **89**, 025004 (2017).
- [44] Z. Ebadi, B. Mirza, and H. Mohammadzadeh, *JCAP* **11**, 057 (2013).
- [45] A.M. Gavrilik, I.I. Kachurik, M.V. Khelashvili, and A.V. Nazarenko, *Physica A: Stat. Mech. Applic.* **506**, 835 (2018).
- [46] A.M. Gavrilik, I.I. Kachurik, and M.V. Khelashvili, *Ukr. J. Phys.* **64**, 1042 (2019).
- [47] A.V. Nazarenko, *Int. J. Mod. Phys. D* **29**, 2050018 (2020).
- [48] E.K. Luckins and R.A. Van Gorder, *Ann. Phys.* **388**, 206 (2018).
- [49] S.-R. Chen, H.-Yu Schive, and T. Chiueh, *MNRAS* **468**, 1338 (2017).
- [50] H.-Yu Schive, T. Chiueh, and T. Broadhurst, *Nat. Phys.* **10**, 496 (2014).
- [51] G.P. Horedt, *Astron. Astrophys.* **160**, 148 (1986).
- [52] L.D. Landau and E.M. Lifshitz, *Statistical Physics* (Pergamon Press, NY, 1978).
- [53] T. Harko, *Eur. Phys. J. C* **79**, 787 (2019).
- [54] A. Kamada, M. Kaplinghat, A.B. Pace, and H.-B. Yu, *Phys. Rev. Lett.* **119**, 111102 (2017).
- [55] R. Lakes and K.W. Wojciechowski, *Phys. Status Solidi* **245**, 545 (2008).
- [56] R. Gatt and J.N. Grima, *Phys. Status Solidi*, **2**, 236 (2008).
- [57] J.A. Kornblatt, E.B. Sirota, H.E. King Jr., H. Baughman, C.-X. Cui, S. Stafstrom, and S.O. Dantas, *Science* **281**, 143 (1998).
- [58] B. Moore, T. Jaglinski, D.S. Stone, and R.S. Lakes, *Philos. Mag. Lett.* **86**, 651 (2007).
- [59] C.-J. Gao, M. Kunz, A.R. Liddle, and D. Parkinson, *Phys. Rev. D* **81**, 043520 (2010).
- [60] O. Luongo and H. Quevedo, *Int. J. Mod. Phys. D* **23**, 1450012 (2014).
- [61] A.M. Scarfone and P. Narayana Swamy, *J. Stat. Mech.: Theory & Experim.* (2009) P02055.
- [62] A.M. Gavrilik, I.I. Kachurik, and Yu.A. Mishchenko, *Ukr. J. Phys.* **56**, 948 (2011).
- [63] A.M. Gavrilik, I.I. Kachurik, and Yu.A. Mishchenko, *J. Phys. A: Math. Theor.* **44**, 475303 (2011).
- [64] A.M. Gavrilik and Yu.A. Mishchenko, *Phys. Lett. A* **376**, 1596 (2012).
- [65] A.M. Gavrilik and Yu.A. Mishchenko, *Ukr. J. Phys.* **58**, 1171 (2013).
- [66] A.M. Gavrilik and Yu.A. Mishchenko, *Nucl. Phys. B* **891**, 466 (2015).
- [67] A.M. Gavrilik and Yu.A. Mishchenko, *Phys. Rev. E* **90**, 052147 (2014).
- [68] S.-Y. Lee, J. Thompson, S. Raeisi, P. Kurzynski, and D. Kaszlikowski, *New J. Phys.* **17** (2015).
- [69] P. Schwaller, *Phys. Rev. Lett.* **115**, 181101 (2015).
- [70] D. Croon, V. Sanz, and G. White, *J. High Energy Phys.* **08** (2018)203.
- [71] M. Bezares and C. Palenzuela, *Class. Quant. Grav.* **35**, 23 (2018).
- [72] A. Bhoonah, J. Bramante, S. Nerval and N.-Q. Song, *Gravitational Waves From Dark Sectors, Oscillating Inflaton, and Mass Boosted Dark Matter*, arXiv: 2008.12306.
- [73] J.-W. Lee, S. Lim, and D. Choi, *BEC dark matter can explain collisions of galaxy clusters*, arXiv: 0805.3827.
- [74] A. Maleki, S. Baghram, and S. Rahvar, *Phys. Rev. D* **101**, 023508 (2020).